Optics Letters

Tunable and controllable multi-channel time-comb absorber based on continuous photonic time crystals

Rui-yang Dong,[1] Shuo Wang,[1] Jia-Hao Zou,[2] and Hai-feng Zhang[2,*]

[1]Bell Honors School, Nanjing University of Posts and Telecommunications, Nanjing 210023, China
[2]College of Electronic and Optical Engineering and College of Flexible Electronics (Future Technology), Nanjing University of Posts and Telecommunications, Nanjing 210023, China
*hanlor@163.com

Received 27 March 2023; accepted 14 April 2023; posted 18 April 2023; published 8 May 2023

To date there have been many studies on multi-channel absorbers for conventional photonic crystals (PCs). However, the number of absorption channels is small and uncontrollable, which cannot satisfy applications such as multispectral or quantitative narrowband selective filters. To address these issues, a tunable and controllable multi-channel time-comb absorber (TCA) based on continuous photonic time crystals (PTCs), is theoretically proposed. Compared with conventional PCs with fixed refractive index (RI), this system forms a stronger local electric field enhancement in the TCA by absorbing externally modulated energy, resulting in sharp multi-channel absorption peaks (APs). Tunability can be achieved by adjusting the RI, angle, and time period unit (T) of the PTCs. Diversified tunable methods allow the TCA to have more potential applications. In addition, changing T can adjust the number of multi-channels. More importantly, changing the primary term coefficient of $n_1(t)$ of PTC_1 can control the number of time-comb absorption peaks (TCAPs) in multi-channels within a certain range, and the mathematical relationship between the coefficients and the number of multiple channels is summarized. This will have potential applications in the design of quantitative narrowband selective filters, thermal radiation detectors, optical detection instruments, etc. © 2023 Optica Publishing Group

https://doi.org/10.1364/OL.491783

The concept of continuous photonic time crystals (PTCs) was first introduced by Wilczek and Shapere in 2012 [1,2]. The refractive index (RI) of conventional photonic crystals (PCs) varies periodically with the spatial position, while the RI of PTCs changes periodically with the increase of time. Subsequently, PTCs inspired many researchers to join this new field. By experimenting, Li *et al*. achieved space-time crystals by using trapped ions in a ring threaded by an Aharonov–Bohm flux in 2012 [3]. Choi *et al*. [4] and Zhang *et al*. [5], utilizing a completely different quantum system, observed remarkable features of the temporal crystal state in their 2017 experiments: driving oscillations of an integer multiple of the period. In theory, PTCs can realize any potential application corresponding to conventional PCs, such as making optical isolators without applied magnetic field, stopping light, and creating a synthetic measurement field for light [6–9]. However, it is very difficult to implement the change of probe signal on a time scale to observe the characteristics of PTCs. In previous years of study, many different solutions were used to construct the PTCs system experimentally [10–12]. The RI of material changing regularly with time can also be realized in reality. For instance, electro-optical materials, piezoelectric materials, and graphene materials can all produce time-varying results of RI.

As a current research hotspot, absorbers are widely employed in solar photovoltaic cells, filters, optical detectors, and biological and chemical sensors [13,14]. For instance, Wu *et al*. introduced a graphene-based hyperbolic metamaterial as the absorbing thin sheet [15]. An array of tungsten wires on top of a silicon nitride substrate was used by Diem *et al*. to show a wide-angle ideal absorber/thermal emitter in the terahertz (THz) regime [16]. Wang *et al*. designed graphene wrapped around one-dimensional PCs separated by a dielectric to excite the optical Tamm state to form a multi-channel absorber [17]. Aly *et al*. did a lot of work on filters, for example, tunable filtering characteristics can be achieved by changing the thickness of the metamaterial layer and the superconductor layer [18]. In addition, to our knowledge, there have been few studies on continuous PTC systems within the last few years. Work on making absorbers with continuous PTC systems—even step-like PTCs—has not yet appeared. Nowadays, work is still in the theoretical stage [19,20] and experimental preparation stage, facing many challenges [21].

Unfortunately, for conventional PCs, the number of absorber channels is small and uncontrollable, which cannot satisfy applications such as multi-spectrum or quantitative narrowband selective filters. In this Letter, a structure based on continuous PTCs is designed to realize a tunable and controllable multi-channel time-comb absorber (TCA) theoretically. The TCA has potential value for plenty of applications.

Firstly, compared with the step-like function model, the continuous PTCs model is given. However, to the best of our knowledge, there is no work on the study of absorbers for step-like PTCs. The step-like function model is proposed in Fig. 1. T_0 indicates the time starting point. T represents a period unit in the time regime, which can be divided into two periods: T_1 and T_2.

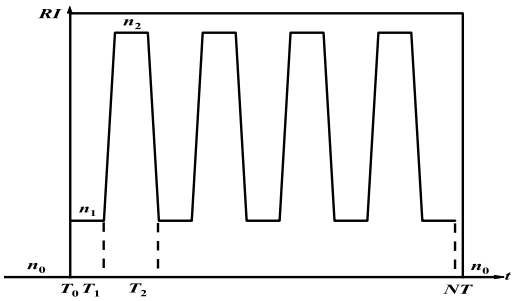

Fig. 1. Discrete model of step-like function in previous investigation [19].

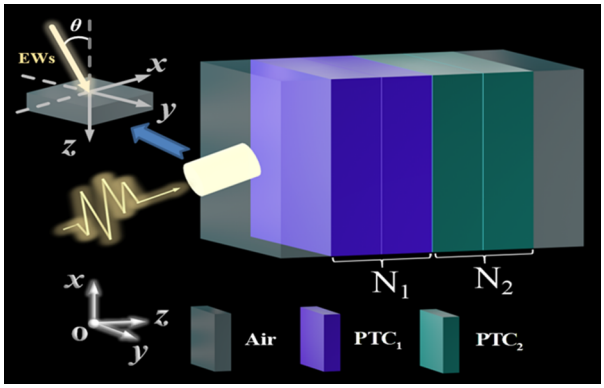

Fig. 2. Derived theoretical models of continuous PTC. The RI of PTC_1 and PTC_2 are $n_1(t) = t^2 + 15t + 0.05$, and $n_2(t) = t + 1.5 - 0.5i$ (where i denotes the imaginary part of the medium), respectively. Periodicity N_1 and N_2 of PTC_1 and PTC_2 are 2. $T = 0.4$ s.

The RI is n_1 in the time period T_1 and n_2 in the time period T_2. When time periodic lattice $t < T_0$ or $t > NT$, the model is placed in a scenario with an RI of n_0, corresponding to $n(t) = n_0$. The RI of the step-like function model is fixed in time periods T_1 and T_2, which is quite different from the proposed continuous model.

The TCA in this Letter is shown in Fig. 2. The entire background space is PTCs material.

The whole TCA of the matrix can be written:

$$M = m_0^{-1}(m_{1j}p_{1j}m_{1j}^{-1}m_{1j+1}p_{1j+1}m_{1j+1}^{-1})^{N1}(m_{2j}p_{2j}m_{2j}^{-1}m_{2j+1}p_{2j+1}m_{2j+1}^{-1})^{N2}m_0 \quad (1)$$

where subscripts 1 and 2 represent the correlation matrix values of PTC_1 and PTC_2, respectively (see Supplement 1, Section 2).

Similar to conventional PCs, there is no reflected wave in the exit space, and the PTCs have a constant RI at the exit time. It means that the electric field of the reflected wave in the exit space $E^-_{Nx} = 0$. The T_r and R of the PTCs are obtained (see Supplement 1, Section 2):

$$Tr = \left|\frac{E^+_{Nx}}{E^+_{0x}}\right|^2 = \left|\frac{1}{M(1,1)}\right|^2 \quad (2)$$

$$R = \left|\frac{E^-_{0x}}{E^+_{0x}}\right|^2 = \left|\frac{M(2,1)}{M(1,1)}\right|^2. \quad (3)$$

The absorptance A is written as follows:

$$A = 1 - Tr - R. \quad (4)$$

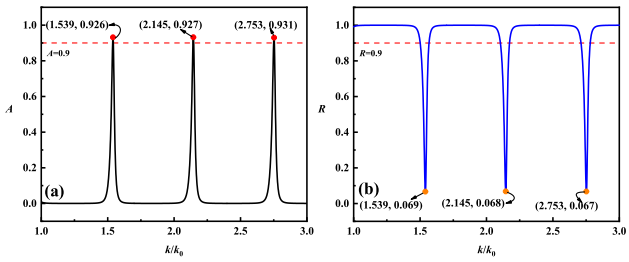

Fig. 3. TCA obtained based on continuous PTC system. (a) A, and (b) R.

Due to the irreversibility of time, the structure containing PTCs is two completely different subsystems for forward propagation and backward propagation. Electromagnetic waves will exhibit completely different properties (see Supplement 1 Section 3). Here, we only discuss the case of forward propagation. At the same time, considering that the current PTC system is still in the experimental preparation stage, it faces the problem of material selection. In this work, the time-comb absorption peaks (TCAPs) of theoretical calculations are all greater than 0.9, and the specific problem of energy loss is no longer considered. Moreover, this work has nothing to do with the sensitivity of the sensor.

The theoretical analysis of the simulation results is presented below. In Fig. 3, the absorption (A) and reflection (R) of the TCAs are plotted. From Fig. 3(a), it can be seen that the TCA multiple channels (MC) is 3 and the values of the TCAPs are greater than 0.9, which has a good absorption performance. The first, second, and third TCAPs are located at $k = 1.539k_0$, $k = 2.145k_0$, and $k = 2.753k_0$ due to the effect of the temporal topological edge state [19,20]. The values of the TCAPs are 0.926, 0.927, and 0.931, respectively. To show the properties of the proposed continuous PTCs more comprehensively, the variation of the R curve with k is given, as shown in Fig. 3(b). What can be seen is that in the k range, where the value of A is zero, the value of R is close to 1, and when A is greater than 0.9, the R curve decreases rapidly at the same k value.

Next, the electric field of the TCA will be drawn to explain the mechanism of the formation of TCAPs. Select the absorption peak (AP) at $k = 2.145k_0$ for plotting. The reason for the extension of the horizontal coordinate time to 1.6 s is that $T = 0.4$ s: while the periodicity N_1 and N_2 of PTC_1 and PTC_2 are each 2, $t = T \times (N_1 + N_2) = 1.6$ s. From Fig. 4, the electric field shows a rapid local enhancement near $t = 0^+$ (right limit of zero), even exceeding the standard value of the normalized electric field 1. As can be seen from the local magnification in Fig. 4, the local enhancement of the electric field almost is 52 times the normalized value. This is an astonishing phenomenon [19,20]. This amazing energy is likely drawn from the external modulation of the RI in a time-varying manner. When the time increases, the electric field appears to fall and rise, creating a local peak in the electric field. The electric field transmitted through the TCA is zero in the range from 0.5 s to1.6 s. This is fully consistent with the above analysis for Fig. 3, which corresponds to a TCA with a transmittance equal to zero.

Then, the effect of θ on the number of MCs is discussed in Fig. 5. In Fig. 5(a), the number of MCs is 3, 3, and 1 when θ is equal to 0°, 30°, and 60°, respectively. In Fig. 5(b), the 3-D top view of A varies with θ, and k is displayed. The white curve

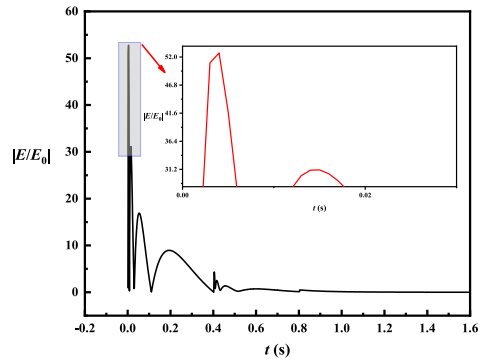

Fig. 4. Electric field distribution of TCA when k is equal to $2.145k_0$.

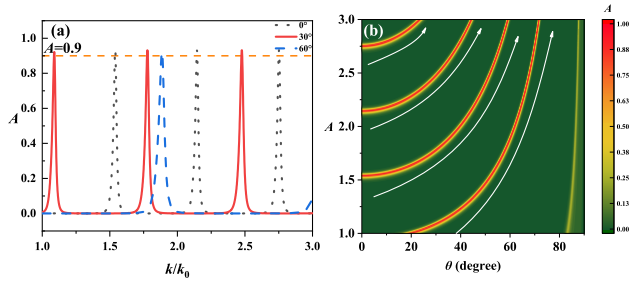

Fig. 5. Effect of θ on the number of MCs. (a) 0°, 30°, and 60°, and (b) the 3-D top view of A varying with θ and k.

indicates the trend of the movement of the TCAPs. It can be clearly seen that as θ increases, the TCAPs move in the direction of higher k. Interestingly, the peak is always greater than 0.9, which means that excellent performance is still maintained. Figure 5(b) can also confirm the phenomenon of Fig. 5(a). In Fig. 5(b), when θ is equal to 0° and 30°, it corresponds to the presence of three peaks represented by the red line; however, when $\theta = 60°$, there is only one peak, represented by the blue-dashed line, which corresponds to the presence of only one AP in the selected k range. Interestingly, there is an angular range where there is no AP from 75° to 82° where the missing AP moves to a higher wave vector range. This will have many potential applications. On the one hand, the full coverage of k in the range of $1k_0 \sim 3k_0$ is achieved based on the change of angle; on the other hand, the excellent performance requirements can still be met even with a wide range of angle changes.

In addition, another interesting phenomenon is that the number of MCs can be tuned by adjusting the RI of PTC_1 and the time period unit T within a certain range. This regulation can be widely used for thermal emissions, directional selection filters, and switches. In Fig. 6, the variation in RI is achieved by changing the value of the primary term coefficient of $n_1(t)$. When the primary term coefficient is varied from 15 to 5 at intervals of 5, it is interesting to find that the number of MCs shows a certain pattern:

$$\mathrm{MC} = 2 \times (20 - \mathrm{A_1})/5 + 1, \tag{5}$$

where A_1 is the primary term coefficient of $n_1(t)$. When A_1 is 15, this corresponds to MC = 3; when A_1 is 10, MC = 5; when A_1 is 5, MC = 7.

The number of channels of this TCA is regularly controlled which can lead to many interesting and valuable practical applications. Unfortunately, the above changes will lose regularity

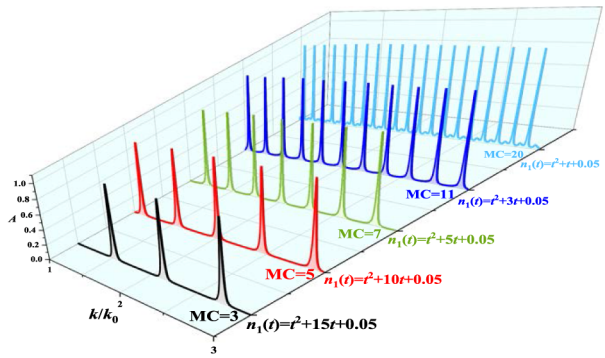

Fig. 6. Effect of $n_1(t)$ of the primary term coefficient on the number of MCs when $n_2(t) = t + 1.5 - 0.5\mathrm{i}$, and $\theta = 0°$.

Table 1. The Number of MCs

A_1	MC	RE
15	3	Yes
10	5	Yes
5	7	Yes
3	11	No
1	20	No

when the coefficient continues to decrease. However, it is worth mentioning that the number of MCs increases rapidly as the coefficient decreases, but still satisfies TCAPs greater than 0.9. The number of MCs corresponding to coefficients of 3 and 1 are 11 and 20, respectively, as shown in Table 1. Considering that when the primary term coefficient of $n_1(t)$ is 5, the corresponding number of MCs is 7, the quantity is moderate at this time. Both the advantages of the TCAPs are demonstrated and the analysis is facilitated. Thus, the subsequent studies are based on $n_1(t) = t^2 + 5t + 0.05$.

Likewise, when the number of MCs increases rapidly, another interesting feature is introduced: tunability. In Fig. 6, as the number of MCs increases, the range of the covered k also expands. This allows the TCA to have excellent frequency tunability.

This is even more evident in Fig. 7. When the time decreases from $T = 0.8$ s to $T = 0.2$ s in 0.2 s intervals, the number of MCs is rapidly increasing, respectively 4, 5, 7, and 12. It can be understood that as time decreases, new TCAPs constantly appear without affecting the TCAPs that were present. The peaks are still all greater than 0.9. The reason for this phenomenon is that when the T change interval decreases, the same size of energy will be more concentrated on a smaller T (this does not mean that the absorbed energy decreases, the absorbed energy mainly depends on the periodic number). Thus, the local enhancement of the electric field will be more pronounced and intense when the system of PTCs absorbs the same amount of energy. The number of TCAPs increases. In summary, the decrease in T leads to an increase in TCAPs.

Considering the constant term of $n_2(t)$ of 0.5, the peak of the AP is the largest. Thus, the following research is based on $n_2(t) = t + 0.5 - 0.5\mathrm{i}$ (see Supplement 1, Section 6).

In Fig. 8, the effect of the imaginary part of $n_2(t)$ on the peak is explored. It can be clearly seen that the effect of the imaginary part on the peak is more direct compared to in Fig. 7. As the imaginary part decreases from 2 to 0.1, the overall trend of the peak increases and then decreases slightly. The peak reaches

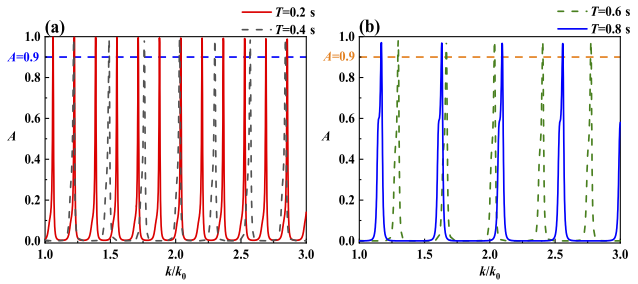

Fig. 7. Effects of t on the number of MCs. (a) $T = 0.2$ s, and $T = 0.4$ s, and (b) $T = 0.6$ s, and $T = 0.8$ s. $\theta = 0°$.

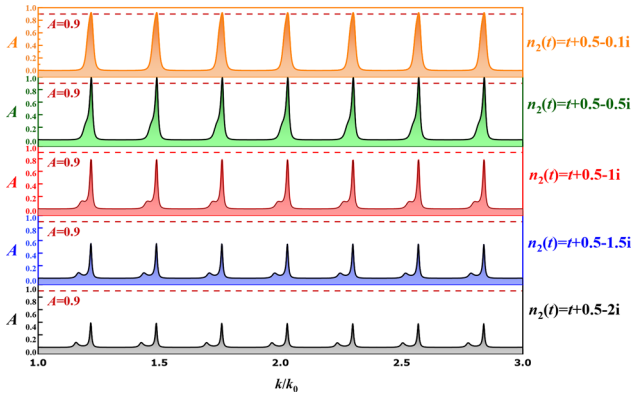

Fig. 8. Effect of imaginary part of $n_2(t)$ on TCAPs from 2 to 0.1 in the case of θ equal to 0°.

its maximum at 0.5i, close to 1. It can be seen that the best performance achieved is 0.5i

Here, the effect of the periodicity of PTC_2 on the number of MCs and the value of TCAP is discussed, which is short for N_2. Given that $N_1 = 2$ has a very good phenomenon (see Supplement 1, Section 7), the effect of N_2 on the performance of the TCA is researched in the case of $N_1 = 2$. In Fig. 9, the influence of N_2 on the TCAPs is very small, generally greater than 0.9. It should be noted that periodicity has no impact on the number of MCs. In Fig. 9, the number of MCs is always equal to 7. In the PTC system, what is produced is not reflection as we usually understand it, but time reflection [19,20]. The increase in periodicity means that more energy is drawn from the external modulation energy, but this energy is used to influence the peak and does not act on the number of MCs.

To sum up, a tunable and controllable multi-channel TCA is proposed based on a structure that is composed of continuous PTCs in theory. The TCA draws on externally modulated energy, such as that which causes the RI of the PTC to vary in time, creating a strong local electric field enhancement inside the TCA. In turn, the final electric field through the TCA is almost zero, resulting in a narrowband, multi-channel TCA. When θ is changed from 0° to 75°, full coverage of the TCAPs in the range of $1k_0 \sim 3k_0$ is achieved for the wave vector. In addition, changing the primary term coefficient of $n_1(t)$ can realize the controllable number of MCs and summarize the law as $MC = 2 \times (20 - A_1)/5 + 1$. The maximum number of channels is 20. When T decreases from 0.8 s to 0.2 s in intervals of 0.2 s, the number of MCs increases, which are 4, 5, 7, and 12, respectively. This is actually a manifestation of tunability. It can

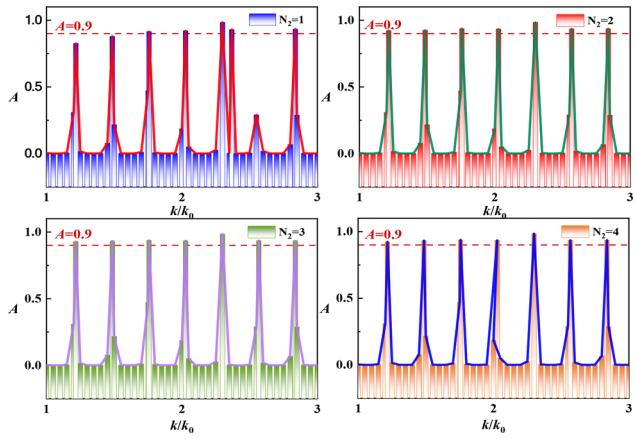

Fig. 9. The impact of N_2 on the number of MCs when $N_1 = 2$, $\theta = 0°$, $n_1(t) = t^2 + 5t + 0.05$, and $n_1(t) = t + 0.5 - 0.5i$, $\theta = 0°$.

be expected that the presented idea has potential applications in quantitative narrowband selective filters, thermal radiation detectors, and electromagnetic wave energy harvesters.

Disclosures. The authors declare no conflicts of interest.

Data availability. Data underlying the results presented in this paper are not publicly available at this time but may be obtained from the authors upon reasonable request.

Supplemental document. See Supplement 1 for supporting content.

REFERENCES

1. F. Wilczek, Phys. Rev. Lett. **109**, 160401 (2012).
2. A. Shapere and F. Wilczek, Phys. Rev. Lett. **109**, 160402 (2012).
3. T. Li, Z. X. Gong, Z. Q. Yin, H. T. Quan, X. Yin, and P. Zhang, Phys. Rev. Lett. **109**, 163001 (2012).
4. S. Choi, J. Choi, R. Landig, G. Kucsko, and H. Zhou, Nature **543**, 221 (2017).
5. J. Zhang, P. W. Hess, A. Kyprianidis, and P. Becker, Nature **543**, 217 (2017).
6. M. F. Yanik and S. Fan, Phys. Rev. Lett. **93**, 173903 (2004).
7. S. Longhi, Phys. Rev. E **75**, 026606 (2007).
8. Z. Yu and S. Fan, Nat. Photonics **3**, 91 (2009).
9. K. Fang, Z. Yu, and S. Fan, Nat. Photonics **6**, 782 (2012).
10. K. Narayanan, A. W. Elshaari, and S. F. Preble, Opt. Express **18**, 9809 (2010).
11. Y. Akihama, Y. Kanamori, and K. Hane, Opt. Express **19**, 23658 (2011).
12. S. Vezzoli, V. Bruno, C. DeVault, T. Roger, V. M. Shalaev, A. Boltasseva, M. Ferrera, M. Clerici, A. Dubietis, and D. Faccio, Phys. Rev. Lett. **120**, 043902 (2018).
13. M. Tonouchi, Nat. Photonics **1**, 97 (2007).
14. S. Thongrattanasiri, F. H. L. Koppens, and F. J. G. de Abajo, Phys. Rev. Lett. **108**, 047401 (2012).
15. J. Wu, L. Jiang, J. Guo, X. Dai, Y. Xiang, and S. Wen, Opt. Express **24**, 17103 (2016).
16. M. Diem, T. Koschny, and C. M. Soukoulis, Phys. Rev. B **79**, 033101 (2009).
17. X. Wang, X. Jiang, Q. You, J. Guo, X. Dai, and Y. Xiang, Photonics Res. **5**, 536 (2017).
18. A. H. Aly and D. Mohamed, J. Supercond. Nov. Magn. **32**, 1897 (2019).
19. E. Lustig, Y. Sharabi, and M. Segev, Optica **5**, 1390 (2018).
20. M. Lyubarov, Y. Lumer, A. Dikopoltsev, and E. Lustig, Science **377**, 425 (2022).
21. S. Saha, O. Segal, C. Fruhling, and E. Lustig, Opt. Express **31**, 8267 (2023).